Grading plasmonic nanoparticles with light

Alexander A. Zharov, Jr.,[1] Alexander A. Zharov,[1] Ilya V. Shadrivov,[2] and Nina A. Zharova[3]
[1]*Institute for Physics of Microstructures, Russian Academy of Sciences, Nizhny Novgorod 603950, Russia and N.I. Lobachevsky State University, Nizhny Novgorod 603950, Russia*
[2]*Nonlinear Physics Centre, Research School of Physics and Engineering, Australian National University, Canberra, Australian Capital Territory 2601, Australia*
[3]*Institute of Applied Physics, Russian Academy of Sciences, Nizhny Novgorod 603950, Russia*
(Received 8 July 2015; published 12 January 2016)

We introduce an approach for fine grading of plasmonic ellipsoidal nanoparticles by two interfering light beams. We consider electrically neutral subwavelength metal nanoparticles whose response is described within the dipole approximation. For the ellipsoidal nanoparticles, we find that their polarizability tensor is strongly dispersive due to the existence of two orthogonal plasmon modes. These modes can be resonantly excited by light and the optical force experienced by particles depends on the ratio of ellipsoid semiaxes. This dependence allows us to spatially separate ellipsoidal particles with different aspect ratio. The eigenfrequencies of plasmons depend on the depolarization factor as well as on the permittivity of the environment and therefore our results can potentially be employed in a wide frequency range including near infrared, visible, and ultraviolet.

DOI: 10.1103/PhysRevA.93.013814

I. INTRODUCTION

Increased interest in the development and application of various nanoparticles requires advanced methods for their manipulation, which is a complex task due to the size of these particles. Finite tolerances in fabrication often lead to the presence of various size particles in the output of the fabrication process. This is why the development of efficient techniques for separation and sorting of nanoparticles and their clusters (e.g., in colloids, living cells, and macromolecules) is of great interest. Proposals of size separation of microparticles using laser radiation date back to 1970 [1], when it was first demonstrated that one can manipulate the dielectric microspheres using laser radiation pressure. Renewed interest in this subject in the past decade has been motivated by advances in nanofabrication technology, which aims to develop new approaches for subwavelength light manipulation and signal processing on the nanoscale.

Previous works have demonstrated that optical manipulation and sorting of submicrometer objects can be realized by means of evanescent wave interference patterns [2], by far-field interference patterns [3], by time-modulated laser radiation [4], and by using Bessel modes and Laguerre-Gaussian beams [5,6]. The underlying mechanism of optical manipulation is defined by ponderomotive forces experienced by particles within the light field. In the simplest case these forces can be represented as a superposition of a scattering force along the beam axis and a gradient force resulting from nonuniform spatial distribution of light intensity (for example, in the vicinity of the beam focus) [7]. In the case of Rayleigh-sized particles (nanoparticles), the dipole approximation method has been successfully applied to calculate the force, giving reasonable agreement with complete Mie theory [8].

The optical forces acting on nanoparticles are quite small since they are proportional to the volume of a particle and this makes manipulation of extremely small particles challenging. This problem can be mitigated in the case of metal nanoparticles by using their plasmonic resonances, when the resonant growth of fields in the vicinity of the particle leads to the enhancement of the ponderomotive forces, including both gradient and scattering components. Resonant plasmonic properties of noble-metal nanoparticles are already used for biomolecular sensors [9], localized heaters [10], photonic imaging [11], and tailoring metamaterial properties [12]. Extensive studies in this area consider mainly size sorting of spherical nanoparticles (see Refs. [13–16]).

Further studies propose the use of the nonspherical particles for force calibration purposes [17]. In the present paper we consider the problem of grading ellipsoidal plasmonic nanoparticles. This problem did not receive appropriate attention in earlier publications. However, the separation of nanoparticles based on their aspect ratio seems to be an important capability that can complement the size-sorting processes in order to be able to extract particles that are highly uniform in both size and shape from the mixtures of various particles.

II. PONDEROMOTIVE FORCES

First, we consider a single small metallic particle surrounded by a viscous medium in an inhomogeneous electromagnetic field. Our first goal is to find the forces acting on this particle. We suppose that the particle is much smaller than the wavelength, hence its response to the external field can be studied within the dipole approximation, when the photophoretic and light pressure forces can be neglected. In contrast, the ponderomotive force does not vanish in the dipole approximation. It consists of two parts: one is the force acting on the dipole in a weakly inhomogeneous electric field and the other is the Lorentz force acting on the polarization current induced by the electromagnetic wave in the particle

$$\boldsymbol{F}_{(PM)} = (\boldsymbol{p}\nabla)\boldsymbol{E} + \frac{1}{c}\left[\frac{\partial \boldsymbol{p}}{\partial t} \times \boldsymbol{B}\right]. \tag{1}$$

We are interested in the averaged particle motion in the high-frequency field $E \sim \exp(i\omega t)$, neglecting fast oscillations, so this motion is defined by the ponderomotive (or Miller [18])

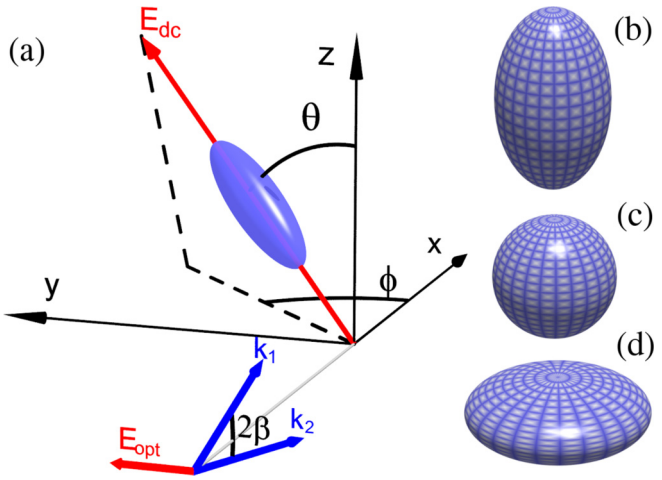

FIG. 1. (a) Schematics of the problem. The particle is oriented along the static electric field. Two optical beams with wave vectors $\mathbf{k}_1$ and $\mathbf{k}_2$ produce optical forces that strongly depend on the shape of the particles. We consider the following ellipsoids of revolution: (b) a prolate ellipsoid, (c) a sphere, and (d) an oblate ellipsoid.

force averaged over the period of the field

$$\langle \boldsymbol{F} \rangle = \tfrac{1}{2}\{(\boldsymbol{p}\nabla)\boldsymbol{E}^* + [\boldsymbol{p} \times \mathrm{curl}\boldsymbol{E}^*] + \mathrm{c.c.}\}, \tag{2}$$

or equivalently

$$F_i = \tfrac{1}{2}(p_k \nabla_i E_k^* + \mathrm{c.c.}), \tag{3}$$

where we sum over the repeating indices. In the linear approximation the electric dipole moment can be expressed as $\boldsymbol{p} = \hat{\alpha}\boldsymbol{E}$, where $\hat{\alpha}$ is a polarizability tensor of a particle. As a particular example we consider a two-dimensional geometry (the field is homogeneous along the y axis) and TE polarization of the electromagnetic wave. In such a case the force can be expressed in the explicit form

$$F_x = \frac{1}{2}\left(\alpha_{yy} E_y \frac{\partial E_y^*}{\partial x} + \mathrm{c.c.}\right), \tag{4}$$

$$F_y = 0, \tag{5}$$

$$F_z = \frac{1}{2}\left(\alpha_{yy} E_y \frac{\partial E_y^*}{\partial z} + \mathrm{c.c.}\right), \tag{6}$$

where x is the axis along the wave vector, while the electric field is directed along the y axis, as shown in Fig. 1(a). We can represent the electric field as $E_y = A(x,z)\exp[-i\,\Phi(x,z)]$, where $A(x,z)$ and $\Phi(x,z)$ are real amplitude and phase, respectively. Then the expression for the force assumes a more compact form

$$\boldsymbol{F} = A^2 \nabla \Psi, \tag{7}$$

with

$$\Psi = \tfrac{1}{2}\mathrm{Re}\alpha_{yy} \ln A^2 - \mathrm{Im}\alpha_{yy}\Phi, \tag{8}$$

where Re and Im stand for real and imaginary parts, respectively. The ponderomotive force (7) can be conventionally split into two parts: gradient force, which is proportional to the real part of the polarizability, and scattering force, which is proportional to the imaginary part of the polarizability. The scattering force is caused by the momentum transfer from absorbed photons to the nanoparticle.

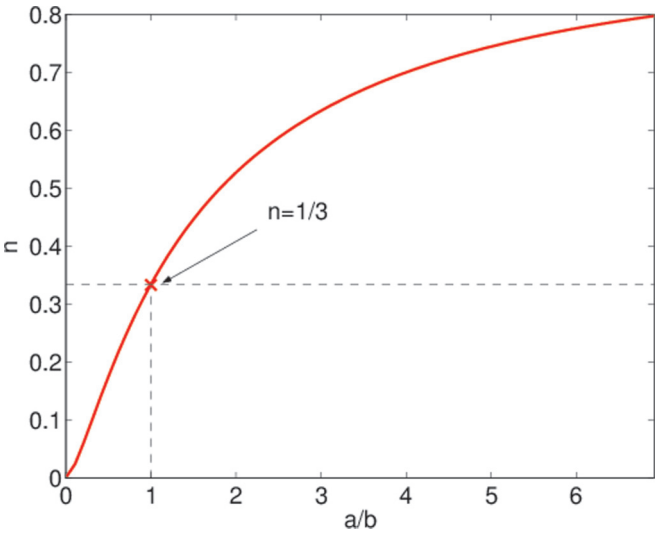

FIG. 2. Depolarization factor n as a function of the ratio of the semiaxes of the ellipsoid of revolution a/b.

III. ELLIPSOIDAL PARTICLES

As an example of the nontrivially shaped nanoparticles we consider ellipsoids of revolution. For nanoparticles of such shape the polarizability can be found in a quasistatic limit and in the principal axes it is defined by a tensor

$$\hat{\alpha}^0 = \begin{pmatrix} \alpha_\perp & 0 & 0 \\ 0 & \alpha_\perp & 0 \\ 0 & 0 & \alpha_\parallel \end{pmatrix} \equiv \alpha_\perp \hat{1} + (\alpha_\parallel - \alpha_\perp)\begin{pmatrix} 0 & 0 & 0 \\ 0 & 0 & 0 \\ 0 & 0 & 1 \end{pmatrix}, \tag{9}$$

where we have explicitly separated the isotropic part. In these expressions

$$\alpha_\perp = \frac{a^2 b}{3}\frac{\varepsilon(\omega) - \varepsilon_l}{\varepsilon_l + [\varepsilon(\omega) - \varepsilon_l](1-n)/2}, \tag{10}$$

$$\alpha_\parallel = \frac{a^2 b}{3}\frac{\varepsilon(\omega) - \varepsilon_l}{\varepsilon_l + [\varepsilon(\omega) - \varepsilon_l]n}, \tag{11}$$

where a and b represent principal semiaxes of the ellipsoid, $\varepsilon(\omega)$ is the permittivity of the material of the particle, and ε_l is the permittivity of the surrounding medium. The value n is a so-called depolarization factor given by [19]

$$n = \frac{1}{2}\left(\frac{a}{b}\right)^2 \int_0^\infty \frac{dx}{(1+x)^{3/2}[x + (a/b)^2]}. \tag{12}$$

We note that n depends only on the ratio of semiaxes a/b, which determines the shape of the ellipsoid. Figure 2 shows the dependence of n on this ratio. There are three distinctive shapes: $0 < n < 1/3$ corresponds to the prolate ellipsoid [see Fig. 1(b)], $n = 1/3$ corresponds to the sphere [shown

in Fig. 1(c)], and $1/3 < n < 1$ corresponds to the oblate (disklike) ellipsoid, shown in Fig. 1(d).

In what follows we consider silver particles and use the permittivity data from the refractive index database [20]. Ellipsoidal metal nanoparticles generally support three quasistatic plasmon modes, two of which are degenerate in the case of the ellipsoid of revolution. We note that the eigenfrequencies of surface plasmons of nanoscale particles may fall in quite a wide frequency range, from ultraviolet down to visible and near infrared, and this depends on the permittivity of the surrounding medium ε_l and on the depolarization factor n. The resonant frequencies can be found from Eqs. (10) and (11) and they correspond to the zeros of the real parts of the denominators.

IV. NANOPARTICLE GRADING BY THE FIELD OF TWO CROSSING LIGHT WAVES

We consider the electromagnetic field created by two identical plane waves propagating at an angle 2β with respect to each other as schematically shown in Fig. 1(a). In addition, we assume that there is a static homogeneous electric field, which is strong enough so that it maintains the orientation of the anisotropic nanoparticles and it does not affect the dynamics of particles in any other way. Optical field can be represented as a standing wave in the z direction and a traveling wave in the x direction

$$\begin{aligned} E_y(x,z) &= \tfrac{1}{2}E_0 e^{-ikx-i\varkappa z} + \tfrac{1}{2}E_0 e^{-ikx+i\varkappa z} \\ &= E_0 \cos \varkappa z \exp(-ikx), \end{aligned} \tag{13}$$

where $\varkappa = k_0\sqrt{\varepsilon_l}\sin\beta$, $k = k_0\sqrt{\varepsilon_l}\cos\beta$, and $k_0 = \omega/c$ is the free-space wave number.

We use the amplitude-phase representation that was introduced before and for $A(x,z)$ and $\Phi(x,z)$ we get, respectively,

$$A^2(x,z) = E_0^2 \cos^2 \varkappa z, \tag{14}$$

$$\Phi(x,z) = -kx. \tag{15}$$

The force components are then found as

$$F_x = -kE_0^2 \mathrm{Im}\alpha_{yy} \cos^2 \varkappa z, \tag{16}$$

$$F_z = -\tfrac{1}{2}\varkappa E_0^2 \mathrm{Re}\alpha_{yy} \sin 2\varkappa z. \tag{17}$$

The principal axes of a particle do not necessarily coincide with x, y, and z since the orientation of the particle is imposed by the direction of the constant electric field and can, in principle, be arbitrary. For example, if the shape of the particle is prolate, it orients with its symmetry (long) axis along the static field. Suppose that the constant electric field is applied in the direction characterized by spherical angles ϕ and θ [see Fig. 1(a)]. Then the polarizability tensor of the prolate particle takes the form

$$\hat{\alpha} = \alpha_\perp \hat{1} + (\alpha_\parallel - \alpha_\perp)\hat{\sigma}(\phi,\theta), \tag{18}$$

with

$$\hat{\sigma}(\phi,\theta) = \begin{pmatrix} \cos^2\phi \sin^2\theta & \sin\phi\cos\phi\sin^2\theta & \cos\phi\sin\theta\cos\theta \\ \sin\phi\cos\phi\sin^2\theta & \sin^2\phi\sin^2\theta & \sin\phi\sin\theta\cos\theta \\ \cos\phi\sin\theta\cos\theta & \sin\phi\sin\theta\cos\theta & \cos^2\theta \end{pmatrix}.$$

The case of an oblate particle is more complicated. Indeed, it orients so that the direction of the maximum of its polarization is along the static field. However, now the maximum of polarization is achieved along the long axis of the disklike particle, which is orthogonal to the symmetry axis (short axis of the oblate ellipsoid). At the same time the direction of the short axis is *indifferently stable* in the plane orthogonal to the dc field and may take any angular position in this plane. Denoting this arbitrary angle by ψ and considering that $\psi = 0$ when the short axis of the oblate ellipsoid lies in the plane formed by the dc electric field and the z axis, we can rewrite the components of the polarizability tensor in the form (18) with

$$\begin{aligned} \hat{\sigma}_{xx} &= (\cos\phi\cos\theta\cos\psi - \sin\phi\sin\psi)^2, \\ \hat{\sigma}_{yy} &= (\cos\theta\sin\phi\cos\psi + \cos\phi\sin\psi)^2, \\ \hat{\sigma}_{zz} &= \sin^2\theta\cos^2\psi, \\ \hat{\sigma}_{xy} &= \hat{\sigma}_{yx} = -(\sin\phi\sin\psi - \cos\theta\cos\psi\cos\phi) \\ &\quad \times (\cos\theta\sin\phi\cos\psi + \cos\phi\sin\psi), \\ \hat{\sigma}_{xz} &= \hat{\sigma}_{zx} = -(\cos\phi\cos\theta\cos\psi - \sin\phi\sin\psi)\sin\theta\cos\psi, \\ \hat{\sigma}_{yz} &= \hat{\sigma}_{zy} = -(\sin\phi\cos\theta\cos\psi + \cos\phi\sin\psi)\sin\theta\cos\psi. \end{aligned}$$

Since in our geometry the forces are only affected by α_{yy}, we write this component explicitly

$$\alpha_{yy}^{\mathrm{prl}} = \alpha_\perp + (\alpha_\parallel - \alpha_\perp)\sin^2\phi\sin^2\theta, \tag{19}$$

$$\alpha_{yy}^{\mathrm{obl}} = \alpha_\perp + (\alpha_\parallel - \alpha_\perp)(\cos\theta\sin\phi\cos\psi + \cos\phi\sin\psi)^2 \tag{20}$$

for prolate and oblate particles, respectively. We can take into account ψ by using one of the following approaches. In the first approach we can assume that ψ takes an arbitrary but fixed value (it is somewhat justified when the additional influence of the high-frequency field is also taken into account). In the second approach we can assume that ψ takes random values due to Brownian motion, it is homogeneously distributed from 0 to π, and in order to calculate polarizability (20) we need to average it over ψ.

Figure 3 shows several typical spectra of the forces acting on silver nanoparticles. The force components $F_{x,z}$ depend on the position z_p of the particle and in our calculations we choose it at the coordinate of the maximum gradient of the field intensity along z for $\lambda = 500$ nm (i.e., $z_p = \pi/\kappa_p$, where $\kappa_p = 2\pi/\lambda\sqrt{\varepsilon_l}\sin\beta$). In what follows we present forces per unit volume calculated for the incident field intensity of 1 W/cm^2. To calculate the full physical force for an arbitrary intensity, the calculated force per unit volume has to be multiplied by the volume of the particle and by the intensity of incident light. For a particle of the size of 10 nm the force magnitude can be estimated as $F \sim 10^{-20}$ N. For both oblate and prolate ellipsoids we observe two resonant peaks that correspond to

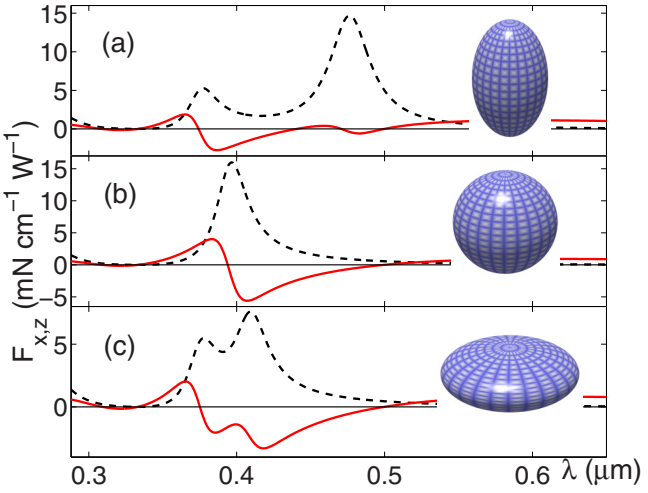

FIG. 3. Optical force components F_x (black dashed line) and F_z (red solid line) as functions of wavelength for different shapes of ellipsoids: (a) $n = 0.2$, (b) $n = 1/3$, and (c) $n = 0.4$. The insets show the schematics of the corresponding particle shapes. Here $\phi = \theta = \pi/4$, $\beta = \pi/6$, and $\psi = \pi/4$. The calculations are made for silver particles. The dielectric permittivity of the viscous medium is $\varepsilon_l = 1.7$ (water) and $z = 382$ nm.

plasmon resonances. For the sphere, when $n = 1/3$, the modes become degenerate and there is only one resonant peak [see Fig. 3(b)]. Two-dimensional color maps in Fig. 4 show force components F_x and F_z as functions of the wavelength and depolarization factor n. We note that the F_x component of the force is always positive, while F_z can change sign, and this is the property that we are going to utilize.

For particle grading purposes, we choose parameters for which the z component of the force changes its sign [corresponding transitions are shown by black contours in Fig. 4(b)]. Near this region of parameter space, particles of slightly different shapes move in opposite directions and get spatially separated provided their depolarization factors are separated by a zero-force boundary. For the calculations presented in Fig. 4, for particles with the shape of an oblate ellipsoid ($n > 1/3$), we use the averaging over the angle ψ as discussed above in order to account for the random orientation of the particles due to their Brownian motion. However, if the short axis direction of the oblate ellipsoid particle can be somehow fixed, then the whole range of behaviors of α_{yy} (and correspondingly $F_{x,z}$) can be realized for identical particles that have different orientation of the short axis ψ. This case is illustrated in Fig. 5, where we show the dependence of the force F_z on n for two orientation angles $\phi = \theta = 0.2\pi$ [Fig. 5(a)] and $\phi = \theta = 0.4\pi$ [Fig. 5(b)] for three different wavelengths. It is clear that the mean value of the force (averaged over ψ) and also the range of possible forces exerted on the particle depend considerably on the orientation of the dc field (i.e., on angles ϕ and θ). As angles ϕ and θ approach $\pm\pi/2$, the forces become larger and so do their gradients. The analysis of the expression (20) shows that for a specific direction of the dc field when it is parallel to the polarization of the optical wave the forces do not depend on ψ and for this very direction the magnitudes of the forces reach their maxima. As a result, we

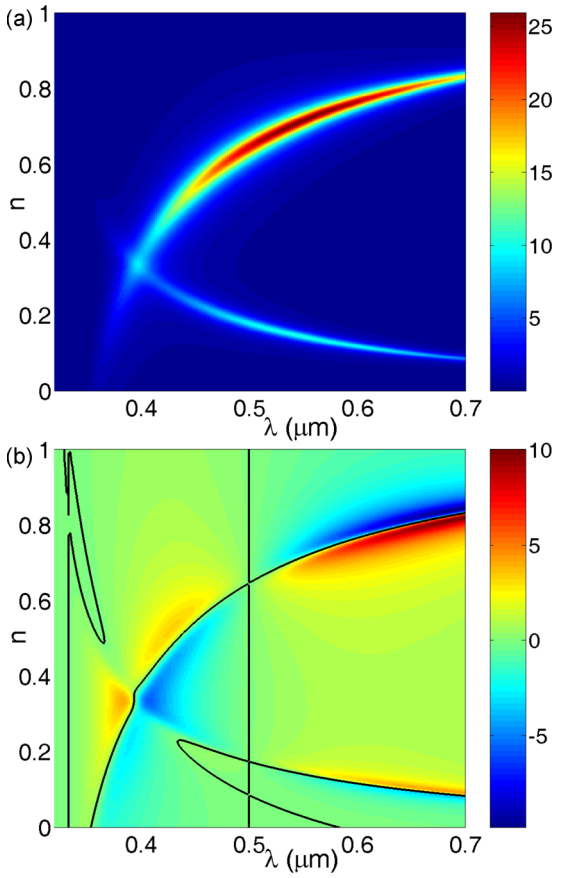

FIG. 4. Components of the optical forces (a) F_x and (b) F_z in units of mN cm^{-1} W^{-1} as a function of wavelength and depolarization factor n. For $n > 1/3$ forces are averaged over ψ as discussed in the text; other parameters are the same as in Fig. 2. The black contour in (b) corresponds to a zero value of F_z.

conclude that this dc field orientation is preferable for sorting the particles.

Material parameters for the particles of sizes of 10 nm and below are different from those found in bulk materials [21,22] since the mean free path of electrons becomes comparable to or larger than the particle size. The permittivity ε_a of a spherical particle of size a is related to the bulk permittivity via

$$\varepsilon_a = \varepsilon_{\text{bulk}} + \frac{\omega_p^2}{\omega^2 + i\omega\gamma} - \frac{\omega_p^2}{\omega^2 + i\omega(\gamma + v_F/a)},$$

where for silver $\hbar\omega_p = 9.1$ eV, $\hbar\gamma = 0.02$ eV [22], v_F is the Fermi velocity of conduction electrons, and $v_F \approx 1.39 \times 10^8$ cm/s. Since our particles are anisotropic with several characteristic sizes, then $1/a$ has to be calculated by averaging the inverse size of the particle over all angles. This averaging is justified due to the isotropic distribution of the Fermi velocity of electrons within the particle. Dashed curves in Fig. 5 show forces calculated for particles whose smaller size is 10 nm, while the larger size is determined via the corresponding depolarization factor n. We see that at shorter wavelengths, the small-size effect broadens the resonances and reduces the magnitude of the forces, while for longer wavelengths the effect is very minor.

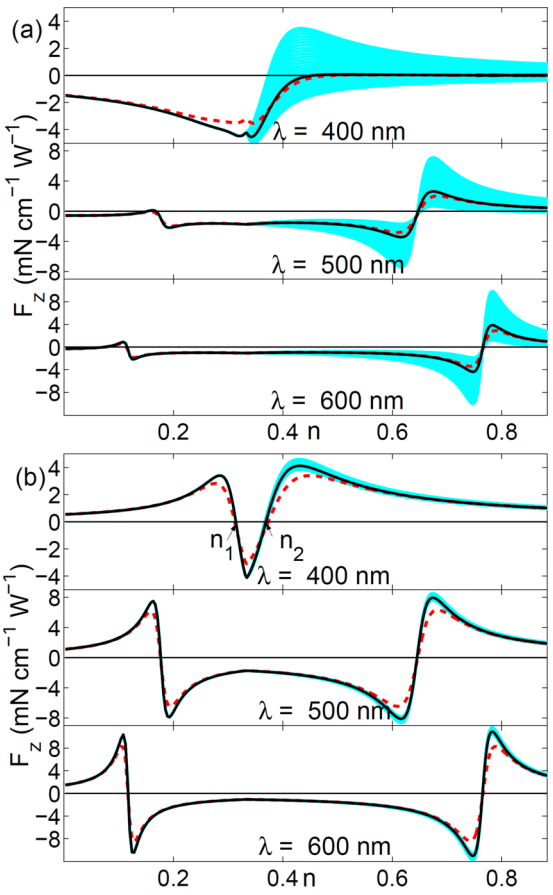

FIG. 5. Dependence of the optical force component F_z on the depolarization factor n for different particle orientations (a) $\phi = \theta = 0.2\pi$ and (b) $\phi = \theta = 0.4\pi$ and different wavelengths $\lambda = 400$, 500, and 600 nm. The force is calculated at maximum intensity gradient in the standing wave, which corresponds to $z_p = 382$, 479, and 575 nm, and $\beta = \pi/6$. Black curves show the mean value of the force averaged over ψ and the cyan (gray) area highlights possible values of F_z that can be achieved by varying ψ. Red dashed curves show forces calculated by taking into account correction to the dielectric permittivity due to the small size of the particles.

To illustrate particle dynamics that can be used for the grading, we plot trajectories of particles of different shapes in Fig. 6. For $n_1 < n < n_2$ particles are attracted to the area of higher field intensity and they are pulled along the x axis by the scattering force. We note that the scattering force does not change the sign and it is always directed along the energy density flow of light. On the other hand, for $n < n_1$ and $n > n_2$ particles are pushed away from the high-intensity gradient region and they stop on the line where $E_y = 0$. Furthermore, the x coordinate of the stopping point also depends on the form of the particle, allowing for even finer grading of particles. The trajectories of the particles are calculated for the same parameters, as force in Fig. 5, where $n_1 \approx 0.3144$, and the corresponding form of the particle is close to spherical. The depolarization factor for the second zero value of force in this case depends weakly on ψ, and $n_2 \approx 0.369$. Even in the low-power regime, when the incident optical power flow is 10 KW/cm^2 we expect that the characteristic velocities acquired by particles near the initial position are of the

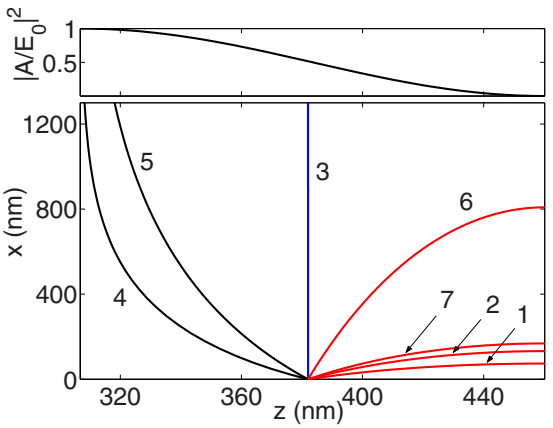

FIG. 6. Shown on the top is the normalized amplitude A/E_0 of the optical wave as a function of z. The bottom shows trajectories of the particles of different shapes. Curves 1–7 correspond to the values of $n_{1,\ldots,7} = (0.2744, 0.2944, \ldots, 0.3944)$. Particles with $0.369 > n > 0.3144$ move to the left (trajectories 4 and 5), in the area of high field, particles with $n \approx 0.3144$ (trajectory 3) do not change z position, and all other particles move to the right. The following parameters were used in calculations: radiation wavelength $\lambda = 400$ nm, $\phi = \theta = 0.4\pi$, $\beta = \pi/6$, and the initial position of particles $z_p = 382$ nm.

order of 1–10 μm/s. This estimation is obtained for particles suspended in water at room temperature.

We note that the dynamics of particles placed in a liquid environment can experience the effect of Brownian motion. As a result, particles will not only move along the described trajectories, but they will also randomly diffuse around these trajectories. To describe this motion we use the Langevin equation, which models random motion of the particle induced by a random force. From the Langevin equation we can find the standard deviation of the particle position from the average as

$$\Delta = \sqrt{\frac{6Bt}{\eta^2}},$$

where $B = kT\eta$, with k the Boltzmann constant, T temperature, and η the coefficient of viscous friction for moving particle, and t is the time of motion. As shown in Fig. 6, particles that are nearly spherical move to the area with higher field intensity and then keep moving along straight lines in the x direction, whereas other particles are trapped in the dark fringes of the interfering waves. In order for separation to work, the time of the spherical particle motion in the x direction should exceed the time that it takes all other particles to stop in the low-intensity region. This condition can be explicitly written as $t > L_\perp/v_{D\perp}$, where $L_\perp$ is the distance that nonspherical particles have to move to their stopping point and $v_{D\perp}$ is the average speed of these particles in the z direction. As a result, the standard deviation can be estimated as

$$\Delta > \sqrt{\frac{6kTL_\perp}{\eta v_{D\perp}}}.$$

Since the friction coefficient is $\eta = F_\perp/v_{D\perp}$, where $F_\perp$ is the force in the z direction, the relative deviation of the particles

can be written as

$$\frac{\Delta}{L_\perp} > \sqrt{\frac{6kT}{F_\perp L_\perp}}. \tag{21}$$

The optical force depends on the light intensity; therefore this condition can be satisfied by choosing an appropriate power. At room temperature in our considered structure, when $L_\perp \sim 500$ nm, the above condition holds for power flows of the order of MW/cm^2 and higher. The Péclet number, which characterizes the ratio between the drift velocity and diffusion velocity, can be written as $F_\perp L_\perp / kT$ and we see that the inverse quantity appears under the square root on the right-hand side of Eq. (21). We see that in order for sorting to work, the Péclet number has to be greater than 6.

V. CONCLUSION

We have shown that optical forces acting on metal nanoparticles strongly depend on the shape of the particles and on their orientation, as well as on the field structure and frequency. We have studied analytically the polarization of particles that have the shape of an ellipsoid of revolution. We found that its polarization can be expressed in terms of a depolarization factor n, which depends on the ratio of ellipsoid semiaxes. Fixing the orientation of ellipsoidal particles by using a static electric field and then illuminating these particles by two interfering light beams, we can create depolarization-factor domains where the gradient ponderomotive force changes sign for ellipsoidal particles with different depolarization factor. Thus, the particles with a different aspect ratio can be moved in opposite directions. This approach allows us to select metal nanoparticles of a particular shape from the mix and extract them. We expect that more complex electromagnetic field patterns can create further possibilities for finer sorting of anisotropic particles of different sizes.

ACKNOWLEDGMENTS

This research was supported in part by the RFBR Grant No. 14-02-00439 and a grant agreement between the Ministry of Education and Science of the Russian Federation and Lobachevsky State University of Nizhni Novgorod, Grant No. 02.B.49.21.0003.

[1] A. Ashkin, Phys. Rev. Lett. **24**, 156 (1970).
[2] T. Cizmar, M. Siler, M. Sery, P. Zemanek, V. Garces-Chavez, and K. Dholakia, Phys. Rev. B **74**, 035105 (2006).
[3] P. Jakl, T. Cizmar, M. Sery, and P. Zemanek, Appl. Phys. Lett. **92**, 161110 (2008).
[4] I. Ricardez-Vargas, P. Rodriguez-Montero, R. Ramos-Garcia, and K. Volke-Sepulveda, Appl. Phys. Lett. **88**, 121116 (2006).
[5] L. Paterson, E. Papagiakoumou, G. Milne, V. Garces-Chavez, S. A. Tatarkova, W. Sibbett, F. J. Gunn-Moore, P. E. Bryant, A. C. Riches, and K. Dholakia, Appl. Phys. Lett. **87**, 123901 (2005).
[6] M. Dienerowitz, M. Mazilu, P. J. Reece, T. F. Krauss, and K. Dholakia, Opt. Express **16**, 4991 (2008).
[7] K. C. Neuman and S. M. Block, Rev. Sci. Instrum. **75**, 2787 (2004).
[8] A. G. Hoekstra, M. Frijlink, L. B. F. M. Waters, and P. M. A. Sloot, J. Opt. Soc. Am. A **18**, 1944 (2001).
[9] G. Raschke, S. Kowarik, T. Franzl, C. Sönnichsen, T. A. Klar, J. Feldmann, A. Nichtl, and K. Kürzinger, Nano Lett. **3**, 935 (2003).
[10] J. Stehr, C. Hrelescu, R. A. Sperling, G. Raschke, M. Wunderlich, A. Nichtl, D. Heindl, K. Kurzinger, W. J. Parak, T. A. Klar, and J. Feldmann, Nano Lett. **8**, 619 (2008).
[11] D. Boyer, P. Tamarat, A. Maali, B. Lounis, and M. Orrit, Science **297**, 1160 (2002).
[12] A. A. Zharov, A. A. Zharov, and N. A. Zharova, J. Opt. Soc. Am. B **31**, 559 (2014).
[13] M. Ploschner, T. Cizmar, M. Mazilu, A. Di Falco, and K. Dholakia, Nano Lett. **12**, 1923 (2012).
[14] K. Dholakia and P. Zemánek, Rev. Mod. Phys. **82**, 1767 (2010).
[15] M. Dienerowitz, M. Mazilu, and K. Dholakia, J. Nanophoton. **2**, 021875 (2008).
[16] M. Ploschner, M. Mazilu, T. F. Krauss, and K. Dholakia, J. Nanophoton. **4**, 041570 (2010).
[17] A. A. M. Bui, A. B. Stilgoe, T. A. Nieminen, and H. Rubinsztein-Dunlop, Opt. Lett. **38**, 1244 (2013).
[18] A. V. Gaponov and M. A. Miller, Zh. Eksp. Teor. Fiz. **34**, 751 (1958) [JETP **7**, 515 (1958)].
[19] L. D. Landau and E. M. Lifshitz, *Electrodynamics of Continuous Media* (Pergamon, Oxford, 1984).
[20] www.refractiveindex.info
[21] H. Hövel, S. Fritz, A. Hilger, U. Kreibig, and M. Vollmer, Phys. Rev. B **48**, 18178 (1993).
[22] F. J. García de Abajo, J. Phys. Chem. C **112**, 17983 (2008).